Article

Journal of Biomedical Nanotechnology
Vol. 10, 393–404, 2014
www.aspbs.com/jbn

Molecular Targeting Radiotherapy with Cyclo-RGDfK(C) Peptides Conjugated to ^{177}Lu-Labeled Gold Nanoparticles in Tumor-Bearing Mice

Andrea Vilchis-Juárez[1,2], Guillermina Ferro-Flores[1,*], Clara Santos-Cuevas[1], Enrique Morales-Avila[2], Blanca Ocampo-García[1], Lorenza Díaz-Nieto[3], Myrna Luna-Gutiérrez[1,2], Nallely Jiménez-Mancilla[1,2], Martha Pedraza-López[3], and Leobardo Gómez-Oliván[2]

[1] *Departamento de Materiales Radiactivos, Instituto Nacional de Investigaciones Nucleares, Carretera México-Toluca S/N, La Marquesa, Ocoyoacac, Estado de México, C.P. 52750, Mexico*
[2] *Universidad Autónoma del Estado de México, Estado de México 50180, Mexico*
[3] *Instituto Nacional de Ciencias Médicas y Nutrición Salvador Zubirán, México D.F., 14000, Mexico*

Peptides based on the cyclic Arg-Gly-Asp (RGD) sequence have been designed to antagonize the function of $\alpha(v)\beta(3)$ integrin, thereby inhibiting angiogenesis. The conjugation of RGD peptides to radiolabeled gold nanoparticles (AuNP) produces biocompatible and stable multimeric systems with target-specific molecular recognition. The aim of this research was to evaluate the therapeutic response of ^{177}Lu-AuNP-RGD in athymic mice bearing $\alpha(v)\beta(3)$-integrin-positive C6 gliomas and compare it with that of ^{177}Lu-AuNP or ^{177}Lu-RGD. The radiation absorbed dose, metabolic activity (SUV, [^{18}F]fluor-deoxy-glucose-microPET/CT), histological characteristics and VEGF gene expression (by real-time polymerase chain reaction) in tumor tissues following treatment with ^{177}Lu-AuNP-RGD, ^{177}Lu-AuNP or ^{177}Lu-RGD were assessed. Of the radiopharmaceuticals evaluated, ^{177}Lu-AuNP-RGD delivered the highest tumor radiation absorbed dose (63.8 ± 7.9 Gy). These results correlated with the observed therapeutic response, in which ^{177}Lu-AuNP-RGD significantly ($p < 0.05$) induced less tumor progression, less tumor metabolic activity, fewer intratumoral vessels and less VEGF gene expression than the other radiopharmaceuticals, a consequence of high tumor retention and a combination of molecular targeting therapy (multimeric RGD system) and radiotherapy (^{177}Lu). There was a low uptake in non-target organs and no induction of renal toxicity. ^{177}Lu-labeled gold nanoparticles conjugated to cyclo-RGDfK(C) demonstrate properties suitable for use as an agent for molecular targeting radiotherapy.

KEYWORDS: *Radiolabeled Gold Nanospheres, RGD Peptides, Lutetium-177, Targeted Radiotherapy.*

INTRODUCTION

Molecular targeting therapy has become a relevant therapeutic strategy for cancer.[1,2] The principle that peptide receptors can be used successfully for *in vivo* targeting of human cancers has been proven, and radiolabeled peptides have been demonstrated to be effective in patients with malignant tumors.[3–5] The effectiveness of targeted radiotherapy depends primarily on the absorbed-dose rate and the total absorbed dose delivered to the tumor and to normal tissues. The dose and its rate depend on the physical properties of the radionuclide, the injected activity and the kinetics of uptake and clearance of radioactivity within the tumor and normal tissue/cells.[6]

Angiogenesis is a physiological process involving the growth of new blood vessels. Angiogenesis is a requirement for tumor growth and metastasis and is stimulated by signal proteins such as the vascular endothelial growth factor (VEGF) and cell adhesion receptors, including integrins. The $\alpha(v)\beta(3)$ integrin, a transmembrane protein consisting of two noncovalently bound subunits (α and β), is over-expressed on activated endothelial cells in the tumor neovasculature and on the cell membrane of various tumor cell types such as ovarian cancer, neuroblastoma, glioblastoma, breast cancer and melanoma cells. Based on

*Author to whom correspondence should be addressed.
Emails: ferro_flores@yahoo.com.mx, guillermina.ferro@inin.gob.mx
Received: 20 March 2013
Accepted: 16 May 2013

the Arg-Gly-Asp (RGD) tripeptide sequence a series of small peptides have been designed to antagonize the function of the $\alpha(v)\beta(3)$ integrin and to inhibit angiogenesis.[7] Radiolabeled RGD peptides have been reported as radiopharmaceuticals with high affinity and selectivity for the $\alpha(v)\beta(3)$ integrin; therefore, these peptides have potential for use in the early detection of rapidly growing tumors and noninvasive visualization of tumor metastasis in cancer patients.[8–12]

Gold nanoparticles can be used to prepare multivalent pharmaceuticals.[13–15] Recently we demonstrated that covalent conjugation of 100 molecules of cyclo-RGDfK(C) to the surface of one radiolabeled gold nanosphere (20 nm, gold-thiol bond) produces a biocompatible and stable multimeric system with target-specific molecular recognition *in vitro* and *in vivo*.[16–19] Due to passive and active-targeting mechanisms, the radiolabeled multimeric and multivalent system exhibit higher tumor uptake than does a RGD-monomer or -dimer.[16, 17]

Lutetium-177 (^{177}Lu) is a radionuclide with a half-life of 6.71 d, a β_{max} emission of 0.497 MeV (78%) and γ radiation of 0.208 MeV (11%) and has been used successfully for radiotherapy with efficient cross-fire effect in cancer cells.[3–5, 20]

If cyclo-RGDfK(C) peptides conjugated to ^{177}Lu-gold nanoparticles (^{177}Lu-AuNP-RGD) are retained in tumors by both passive and active-targeting mechanisms, the total dose (RGD and ^{177}Lu molecules) delivered to the tumor would be significantly higher than that produced by ^{177}Lu-AuNP or ^{177}Lu-RGD, reducing the tumor angiogenic activity and increasing the effectiveness of molecular targeting radiotherapy.

The aim of this research was to evaluate the therapeutic response of ^{177}Lu-AuNP-RGD in athymic nude mice bearing $\alpha(v)\beta(3)$-integrin-positive C6 gliomas and compare the radiation absorbed dose, metabolic activity, histological characteristics and VEGF gene expression in tumor tissues following treatment with ^{177}Lu-AuNP-RGD, ^{177}Lu-AuNP or ^{177}Lu-RGD.

METHODS

Design and Synthesis of ^{177}Lu-DOTA-GGC-AuNP-c[RGDfK(C)](^{177}Lu-AuNP-RGD)

In the c[RGDfK(C)] molecule, the sequence-Arg-Gly-Asp-(-RGD-) acts as the active biological site, the D-Phe (f) and Lys (K) residues complete the cyclic and pentapeptide structure, and Cys (C) is the spacer and active thiol group that interacts with the gold nanoparticle surface (Fig. 1). The c[RGDfK(C)] was synthesized and characterized according to the method described by Morales-Avila et al.[16] In the DOTA-GGC (1,4,7,10-tetraazacyclododecane-N',N'',N'''-tetraacetic-Gly-Gly-Cys) molecule, the GG sequence is the spacer, cysteine (active thiol group) is used to interact with the gold nanoparticle surface and DOTA is used as the lutetium-177 chelator (Fig. 1). The DOTA-GGC was synthesized and characterized according to the method described by Luna-Gutierrez et al.[17]

Gold nanoparticles (AuNP) in injectable-grade water (20 ± 2 nm, 7×10^{11} particles/mL) were synthesized as described by Ocampo-García et al.[19]

Preparation of ^{177}Lu-DOTA-GGC: A 5 μL aliquot of DOTA-GGC (1 mg/mL) was diluted with 40 μL of 1 M acetate buffer at pH 5, followed by the addition of 10 μL of a $^{177}LuCl_3$ ($\sim$740 MBq, $>$ 3 TBq/mg, ITG Isotope Technologies Garching GmbH, Germany) solution. The mixture was incubated at 90 °C in a block heater for 30 min. All solutions were prepared using deionized water. A radiochemical purity of $>$ 98% was verified by TLC silica gel plates (aluminum backing, Merck); 10-cm strips were used as the stationary phase, and ammonium hydroxide:methanol:water (1:5:10) was used as the mobile phase to determine the amount of free ^{177}Lu ($R_f = 0$) and ^{177}Lu-DOTA-GGC ($R_f = 0.4$–0.5). Radiochemical purity was also determined by reversed-phase HPLC on a C-18 column (μ-Bondapack C-18, Waters) using a Waters Empower system with an in-line radioactivity detector and a gradient of water/acetonitrile containing 0.1% TFA from 95/5 (v/v) to 20/80 (v/v) over 35 min at a flow rate of 1 mL/min ($^{177}LuCl_3$ $t_R = 3$–4 min; ^{177}Lu-DOTA-GGC $t_R = 12$–13 min).

Preparation of ^{177}Lu-DOTA-GGC-AuNP-c[RGDfK(C)]: To 1 mL of AuNP (20 nm), 0.025 mL of c[RGDfK(C)] (5 μM; 108 molecules per 20 nm nanoparticle) was added, followed by 3 μL (40 MBq) of ^{177}Lu-DOTA-GGC (0.25 μg of peptide; 1.89×10^{14} molecules; 270 molecules per 20 nm AuNP), and the mixture was stirred for 5 min to form the ^{177}Lu-DOTA-GGC-AuNP-c[RGDfK(C)] system (Fig. 1). No further purification was required because we have found that the maximum number of peptides that can be bound to one AuNP (20 nm) is between 520 and 1701 depending of the peptide structure.[16, 19] The number of peptides per nanoparticle was calculated by UV-Vis titration of peptides (8 μM) using increasing gold nanoparticle concentration (from 0 to 1 nM).[16, 19]

Radiochemical Purity of ^{177}Lu-AuNP-RGD: Size-exclusion chromatography and ultrafiltration were used as radiochemical control methods for the final radiopharmaceutical solution. A 0.1 mL sample of ^{177}Lu-DOTA-GGC-AuNP-c[RGDfK(C)] was loaded onto a PD-10 column and injectable water was used as the eluent. The first radioactive and red eluted peak (3.0–4.0 mL) corresponded to radiolabeled AuNP-c[RGDfK(C)]. The free radiolabeled peptide (^{177}Lu-DOTA-GGC) appeared in the fraction that eluted at 5.0–7.0 mL, and $^{177}LuCl_3$ remained trapped in the column matrix. Upon ultrafiltration (Centricon YM-30 regenerated cellulose 30,000 MW cut off, Millipore, Bedford, MA, USA), the ^{177}Lu-DOTA-GGC-AuNP-c[RGDfK(C)] remained in the filter, while free ^{177}Lu-DOTA-GGC and $^{177}LuCl_3$ passed through the filter. In the radio-HPLC size exclusion system (ProteinPak 300SW, Waters, 1 mL/min, injectable water),

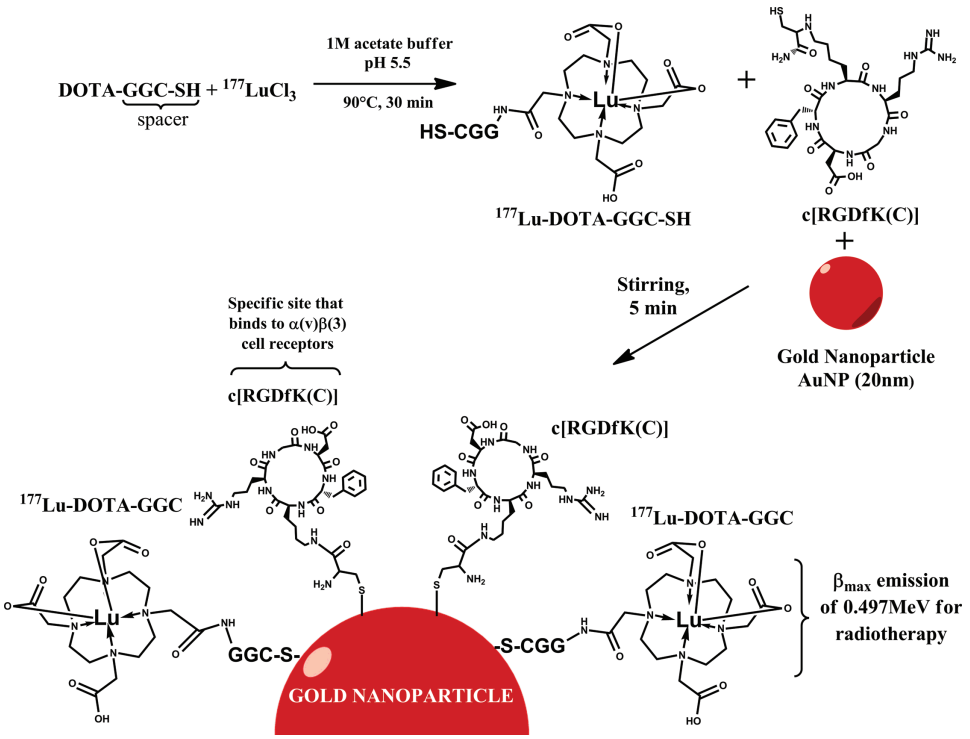

Figure 1. **Overall scheme of ^{177}Lu-DOTA-GGC-AuNP-c[RGDfK(C)] (^{177}Lu-AuNP-RGD) preparation.**

the $t_R s$ for the ^{177}Lu-DOTA-GGC-AuNP-c[RGDfK(C)] and ^{177}Lu-DOTA-GGC were 4–5 and 8 min, respectively (Fig. 2). Chromatographic profiles were obtained using two different detector systems, the UV-Vis detector and a radiometric detector. The sample first passed by the UV-Vis detector (photodiode array) and after 0.37 min (0.37 mL, 1 mL/min) it passed by the radioactive detector. Correspondence of retention times of the peaks of interest in the chromatogram is commonly accepted as a proof of the chemical identity of the radiopharmaceutical. The UV-Vis spectrum, assigned to the peak at 4–5 min using the photodiode array of the system, exhibited the AuNP surface plasmon band at 521 nm. Minor peaks corresponded to minor ^{177}Lu-AuNP-RGD-sizes. (Fig. 2).

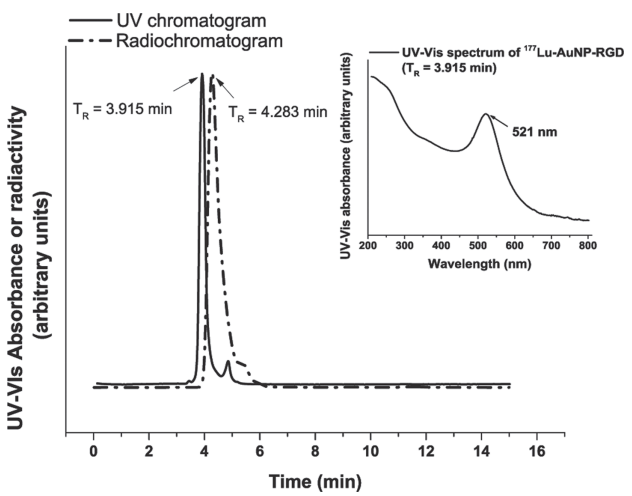

Figure 2. **Size-exclusion HPLC chromatogram (520 nm; continuous line) and HPLC radiochromatogram (dotted line) of the ^{177}Lu-DOTA-GGC-AuNP-c[RGDfK(C)] (^{177}Lu-AuNP-RGD) conjugate. UV-Vis spectrum of the compound with retention time at 3.915 min (inset).**

Preparation of ^{177}Lu-DOTA-GGC-AuNP (^{177}Lu-AuNP)

Three μL (40 MBq) of ^{177}Lu-DOTA-GGC (0.25 μg of peptide; 1.89×10^{14} molecules; 270 molecules per 20 nm AuNP) was added to 1 mL of AuNP (20 nm), and the mixture was stirred for 5 min to form the ^{177}Lu-DOTA-GGC-AuNP system. No further purification was performed. Radiochemical purity was evaluated as described above for ^{177}Lu-AuNP-RGD.

Chemical Characterization

The characterization of the DOTA-GGC and c[RGDfK(C)] conjugated to the gold nanoparticle surface by far infrared (FIR), UV-Vis, X-ray photoelectron spectroscopy (XPS) and Raman spectroscopy was previously reported in detail.[16–19]

Transmission Electron Microscopy (TEM): AuNP, ^{177}Lu-AuNP and ^{177}Lu-AuNP-RGD were characterized in size and shape by TEM using a JEOL JEM 2010 HT microscope operated at 200 kV. The samples were prepared for analysis by evaporating a drop of the aqueous product onto a carbon-coated TEM copper grid.

Particle size and zeta potential: AuNP, ^{177}Lu-AuNP or ^{177}Lu-AuNP-RGD were measured ($n = 5$) using

the particle size (dynamic light scattering = DLS) and *Z* potential Nanotrac-analyzer (Nanotrac Wave, Model MN401, Microtract, FL, USA).

Preparation of ^{177}Lu-DOTA-E-c(RGDfK)$_2$ (^{177}Lu-RGD)

DOTA-E-c(RGDfK)$_2$ was synthesized by Peptide International Inc. (Kentucky, USA) with a purity of > 98% as analyzed by reversed-phase HPLC (RP-HPLC) and mass spectroscopy. A 5 μL aliquot of DOTA-E-c(RGDfK)$_2$ (1 mg/mL) was diluted with 50 μL of 1 M acetate buffer at pH 5, followed by the addition of 10 μL of the ^{177}LuCl$_3$ (~ 370 MBq, > 3 TBq/mg, ITG Isotope Technologies Garching GmbH, Germany) solution. Each mixture was incubated at 90 °C in a block heater for 30 min and diluted to 18 mL with injectable-grade water. A radiochemical purity of > 98% was verified by TLC and HPLC as described above for ^{177}Lu-DOTA-GGC.

Cell Culture

The C6 rat cell line was originally obtained from ATCC (Atlanta, GA, USA). The cells were routinely cultured at 37 °C, with 5% CO_2 and 85% humidity in minimum essential medium eagle (MEM, Sigma-Aldrich Co., Saint Louis, Missouri, USA) supplemented with 10% fetal bovine serum and antibiotics (100 units/mL penicillin and 100 μg/mL streptomycin).

Solid-Phase $\alpha(v)\beta(3)$ Binding Assay

Microtiter 96-well vinyl assay plates (Corning, NY, USA) were coated with 100 μL/well of purified human integrin $\alpha(v)\beta(3)$ solution (150 ng/mL, Chemicon-Millipore Corporation, Billerica, MA, USA) in coating buffer (25 mM Tris-HCl, pH 7.4, 150 mM NaCl, 1 mM $CaCl_2$, 0.5 mM $MgCl_2$ and 1 mM $MnCl_2$) for 17 h at 4 °C. The plates were washed twice with binding buffer (0.1% bovine serum albumin (BSA) in coating buffer). The wells were blocked for 2 h with 200 μL of blocking buffer (1% BSA in coating buffer). The plates were washed twice with binding buffer. Then, 100 μL of binding buffer containing 10 kBq of ^{177}Lu-AuNP-RGD or ^{177}Lu-RGD and appropriate dilutions of c(RGDfK) (from 10,000 nM to 0.001 nM in binding buffer, Bachem-USA) were incubated in the wells at 37 °C for 1 h. After incubation, the plates were washed three times with binding buffer. The wells were cut out and counted in a gamma counter. The IC_{50} values of the RGD peptides were calculated by nonlinear regression analysis ($n = 5$).

In Vitro Cell Proliferation After ^{177}Lu-AuNP-RGD, ^{177}Lu-AuNP and ^{177}Lu-RGD Treatments

C6 cells suspended in fresh medium were incubated in a 96-well plate at a density of 1×10^3 cells/well. The cells were cultured for 24 h at 37 °C with 5% CO_2 and 85% humidity. The growth medium was removed, and the cells were exposed for 2 h (at 37 °C, with 5% CO_2 and 85% humidity) to one of the following treatments ($n = 6$):

(a) 100 μL of ^{177}Lu-AuNP-RGD (5 kBq) and 100 μL of PBS, pH 7,
(b) 100 μL of ^{177}Lu-AuNP (5 kBq) and 100 μL of PBS, pH 7,
(c) 100 μL of ^{177}Lu-RGD (5 kBq) and 100 μL of PBS, pH 7 or
(d) no treatment.

After 2 h, the solution in each well was removed and replaced with fresh culture medium. The cells were maintained for 3 days at 37 °C with 5% CO_2 and 85% humidity. After that, the percentage of cell proliferation in each well was evaluated by the spectrophotometric measurement of cell viability as a function of mitochondrial dehydrogenase activity, which involves the cleavage of the tetrazolium ring of XTT (sodium 3′-[1-[phenylaminocarbonyl]-3,4-tetrazolium]-bis[4-methoxy-6-nitro]benzene sulfonic acid hydrate) in viable cells to yield orange formazan crystals that are dissolved in acidified isopropanol (XTT kit, Roche Diagnostics GmbH, Mannheim, Germany). The resulting absorbance of the orange solution was measured at 480 nm in a microplate absorbance reader (EpochTM, BioTek, VT, USA). The absorbance of the untreated cells was considered as 100% of living C6 cells (or 100% proliferation).

Induction of C6 Tumors in Athymic Mice

Tumor uptake studies in mice were performed according to the rules and regulations of the Official Mexican Norm 062-ZOO-1999. The study was approved by the Institutional Committee for the Care and Use of Laboratory Animals ("*Instituto Nacional de Ciencias Médicas y Nutrición Salvador Zubirán*").

Athymic male mice (20–22 g) were kept in sterile cages with bedding of wood-shavings, constant temperature, humidity, noise and 12:12 light periods. Water and feed (standard PMI 5001 feed) were given *ad libitum*.

Glioma tumors were induced by subcutaneous injection of C6 cells (1.5×10^6) suspended in 0.2 mL of phosphate-buffered saline into the upper back of twenty 6–7-week-old nude mice. Injection sites were observed at regular intervals for tumor formation and progression.

Therapeutic Protocol

Four groups ($n = 5$, total mice = 20) of athymic nude mice bearing C6 gliomas (tumor size 0.05 ± 0.01 g) were used. Each group was treated with one of the following radiopharmaceuticals: (a) ^{177}Lu-AuNP-RGD or (b) ^{177}Lu-AuNP or (c) ^{177}Lu-RGD. There was an untreated control group. All radiopharmaceuticals (four administrations of 2 MBq/0.05 mL; in the case of ^{177}Lu-AuNP-RGD and ^{177}Lu-RGD ~ 3×10^{12} molecules of c-RGD) were injected intratumorally in mice under 2% isoflurane anesthesia. Doses were administered at day 1, 7, 14 and 21, for a total of four doses. Tumor growth was monitored weekly, the

length (L) and width (a) were measured with calipers and the volume was determined as $V = \pi/6 * (L) \times (a^2)$. Considering a tumor density of 1 g/cm^3, the tumor mass in grams was calculated. After 23 days, the mice were sacrificed and tumors and kidneys were dissected and prepared for histopathological or PCR studies as described below. Blood samples were also obtained for creatinine and urea quantification.

Biokinetic Studies

To evaluate biokinetics, the radiopharmaceuticals ^{177}Lu-AuNP-RGD, ^{177}Lu-AuNP or ^{177}Lu-RGD were administered intratumorally in mice with induced C6 tumors (0.05 mL, ~2 MBq). Mice were sacrificed at 3, 24, 48 and 96 h post-administration ($n = 3$ at each time, total mice = 12). Whole liver, heart, spleen, lung, kidneys and tumor as well as samples of blood, intestines, bone and muscle were placed into pre-weighed plastic test tubes. The activity was determined in a well-type scintillation detector (Auto In-V-tron 4010, Nuclear Medical laboratories Inc., CA, USA) along with 3×0.05 mL aliquots of the standard (~2 MBq) representing 100% of the injected dose to obtain the activity corrected by decay. Mean activities were used to obtain the percentage of the injected dose per organ (%ID). The time activity curves corrected by decay $[q_h(t) = A_h(t)e^{\lambda}R^t]$ (biological behavior) for ^{177}Lu-AuNP-RGD, ^{177}Lu-RGD or ^{177}Lu-AuNP were calculated using the %ID at different times.

Radiation Absorbed Dose Assessment

The $A_h(t)$ functions $[A_h(t) = q_h(t)e^{-\lambda_{\mathrm{Lu-177}}t}]$ obtained from the biokinetics studies were integrated to obtain the total number of disintegrations (N) in the main source regions (liver, spleen, kidneys and tumor) during the entire treatment:

$$N_{\mathrm{source}} = \int_{t=0}^{t=23\ \mathrm{d}} A_h(t)\,dt + \int_{t=7\ \mathrm{d}}^{t=23\ \mathrm{d}} A_h(t)\,dt + \int_{t=14\ \mathrm{d}}^{t=23\ \mathrm{d}} A_h(t)\,dt + \int_{t=21\ \mathrm{d}}^{t=23\ \mathrm{d}} A_h(t)\,dt$$

The absorbed dose to organs was evaluated according to the general equation:

$$\bar{D}_{\mathrm{target}\leftarrow\mathrm{source}} = \sum_{\mathrm{sources}} N_{\mathrm{source}} \times DF_{\mathrm{target}\leftarrow\mathrm{source}}$$

where $\bar{D}_{\mathrm{target}\leftarrow\mathrm{source}}$ is the mean absorbed dose to a target organ from a source organ and $DF_{\mathrm{target}\leftarrow\mathrm{source}}$ is a dose factor:

$$DF_{\mathrm{target}\leftarrow\mathrm{source}} = \sum_i \Delta_i \Phi_{i(\mathrm{target}\leftarrow\mathrm{source})}$$

The Δ_i terms are the mean energy emitted per disintegration for the various i-type radiations (i-type emissions, $\sum n_i E_i$). The Φ_i terms are the absorbed fractions that depend on the properties of the i-type emission and the size, shape and separation of the source and target organs. DF values were calculated according to Miller et al.[21] using the beta-absorbed fractions in a mouse model calculated by two Monte Carlo radiation transport codes, MCNP4C and PEREGRINE (voxel-based).

^{177}Lu-SPECT/CT Imaging

Single photon emission computed tomography (SPECT) and X-ray computed tomography (CT) images were acquired 24 h after the last injection (at 22 days of treatment) using a micro-SPECT/CT scanner (Albira, ONCOVISION, Spain) to verify the tumor uptake of ^{177}Lu-AuNP-RGD, ^{177}Lu-AuNP or ^{177}Lu-RGD. Mice under 2% isoflurane anesthesia were placed in the prone position and whole body imaging was performed. The micro-SPECT field of view was 60 mm, a symmetric 20% window was set at 208 keV and pinhole collimators were used to acquire a 3D SPECT image with a total of 64 projections of 30 s, over 360°. The image dataset was then reconstructed using the ordered subset expectation maximization (OSEM) algorithm with standard mode parameter as provided by manufacturer. CT parameters were 35 kV sure voltage, 700 μA current and 600 micro-CT projections.

Standardized Uptake Value (SUV) of [^{18}F]FDG in Tumors with PET/CT: Tumor Metabolic Activity

[^{18}F]FDG (2-deoxy-2-[^{18}F]fluoro-D-glucose)-positron emission tomography (PET) and X-ray CT imaging were performed using a micro-PET/CT scanner (Albira, ONCOVISION, Spain). The images were acquired at the end of the treatments (after 23 days). The micro-PET field of view was 60 mm. Mice were injected in the lateral tail vein with 9 MBq of [^{18}F]FDG in 100 μL PBS under 2% isoflurane anesthesia. After a resting period of 1 h the mice were transferred to the scanning room, placed in a prone position and the whole body imaging was performed. The PET acquisition time was 7.5 min. The CT parameters were those described above. From the [^{18}F]FDG dose and weight of each mouse, the mean standardized uptake value ($n = 5$) [mean SUV = (Bq/g)/(injected activity, Bq/body weight, g)] was calculated using PMOD Data Analysis Software (PMOD technologies).

Creatinine, Urea and BUN Quantification

Blood samples obtained at the end of the treatments were used to quantify creatinine, urea and urea nitrogen (BUN) in order to evaluate kidney function because renal toxicity is the primary obstacle to radiopeptide therapy.[22] Creatinine was measured titrimetrically using the conventional picrate method. Serum urea and BUN were quantified by an enzymatic *in vitro* assay using the coupled urease/glutamate dehydrogenase (GLDH) enzyme system.

Histopathological Evaluation

Tumors and kidneys samples were fixed in neutral 10% formaldehyde for 24 h, washed in 70% ethanol and

Table I. Primers and probes used in the VEGF gene expression assessment in tumor tissues by real time-PCR analysis.

Gen/Accession number	Upper primer	Lower primer	Amplicon (nt)	Probe number*
β-Actin/NM_031144.2	tgccctagacttcgagcaag	ggcagctcatagctcttctcc	72	69
VEGF/AY702972.1	cggagagcaacgtcactatg	tggtctgcattcacatctgc	104	4

Note: *From the universal probe library (Roche).

embedded in paraffin. Sections of 4 μm thickness were placed on slides and dried in an oven at 37 °C. Sections were dewaxed in xylene, rehydrated in a series of graded alcohols, and finally stained with Meyer's hematoxylin/eosin and coverslipped.

Evaluation of VEGF Expression in Tumors by Real-Time PCR

All the oligonucleotides for real-time polymerase chain reaction (qPCR) assays were obtained from Invitrogen (CA, USA). The TaqMan Master reaction, TaqMan probes, capillaries and the reverse transcription (RT) system were from Roche (Roche Applied Science, IN, USA).

Excised tumors were homogenized in 1 mL of Trizol reagent with a Polytron homogenizer (BioSpec Products, Inc.). Total RNA was then extracted following the manufacturer's instructions. Three μg of total RNA was reverse transcribed with the Transcriptor RT system. Real-time PCR was performed with the LightCycler® 2.0 from Roche (Roche Diagnostics, Mannheim, Germany), according to the following protocol: activation of Taq DNA polymerase and DNA denaturation at 95 °C for 10 min, followed by 45 amplification cycles consisting of 10 s at 95 °C, 30 s at 60 °C, and 1 s at 72 °C. Primers sequences, corresponding probe numbers and the sizes of the resulting amplicons are given in Table I. Gene expression of the housekeeping gene β-actin was used as an internal control and the results were expressed as a relative concentration (RC) of β-actin expression.

Statistical Analysis

Differences between the treatment groups were evaluated with Student's t-test. (Significance was defined as $p < 0.05$.)

RESULTS

Chemical Characterization and *In Vitro* Evaluation

^{177}Lu-AuNP-RGD, ^{177}Lu-RGD and ^{177}Lu-AuNP were obtained with radiochemical purities of $> 92\%$. The TEM images of ^{177}Lu-AuNP-RGD and ^{177}Lu-AuNP showed monodisperse solutions (Fig. 3). The increase in the hydrodynamic diameter of the particle by the peptide conjugation-effect was observed by TEM as a low electronic density around the gold nanoparticle due to the poor interaction of the electron beam with the peptide molecules (low electron density), in contrast to the strong scattering of the electron beam when it interacted with the metallic nanoparticles (Fig. 3). The average particle hydrodynamic diameters determined by DLS were 26.6 ± 8.7 nm, 25.6 ± 9.4 nm and 23.8 ± 7.6 nm for ^{177}Lu-AuNP-RGD, ^{177}Lu-AuNP and AuNP, respectively (Fig. 3). The Z potential of ^{177}Lu-AuNP-RGD was -64.6 ± 2.8 mV and that of ^{177}Lu-AuNP was -56.9 ± 3.1 mV, versus -22.2 ± 1.7 mV for the AuNP, indicating that the peptide functionalization (both, DOTA-GGC and c[RGDfK(C)]) conferred a high colloidal stability to the nanosystem.[23]

The *in vitro* affinity, which was determined by a competitive binding assay, indicated that the concentration of c(RGDfK) required to displace 50% of the ^{177}Lu-AuNP-RGD ($IC_{50} = 10.2 \pm 1.1$ nM) or ^{177}Lu-RGD ($IC_{50} = 5.3 \pm 0.4$ nM) from the receptor was the same order of magnitude for both, demonstrating a high *in vitro* affinity for the $\alpha(v)\beta(3)$ integrin for both conjugates. However, the amount of c(RGDfK) required to displace ^{177}Lu-AuNP-RGD from the $\alpha(v)\beta(3)$ protein was twice of that necessary to displace ^{177}Lu-RGD, which may be attributed to the multivalent effect of the AuNP system.[8, 9, 24]

As shown in Figure 4, ^{177}Lu-AuNP-RGD significantly inhibited C6 cell proliferation ($3.62 \pm 1.07\%$) with respect to that of ^{177}Lu-AuNP ($6.32 \pm 1.16\%$) and ^{177}Lu-RGD ($29.67 \pm 2.82\%$), which was also attributed to the greater *in vitro* C6 cell internalization as a result of multivalency.

Biokinetics, Radiation Absorbed Dose and Therapeutic Response

After each of the four intratumoral administrations, the mean tumor uptakes 3 h post injection were $68.1 \pm 7.1\%$ ID (^{177}Lu-AuNP-RGD), $48.2 \pm 5.5\%$ ID (^{177}Lu-AuNP) and $26.8 \pm 2.9\%$ ID (^{177}Lu-RGD), with a high tumor retention for the radiolabeled nanoparticles. The tumor retention of ^{177}Lu-AuNP-RGD at 96 h ($34.7 \pm 4.3\%$ ID) was significantly higher ($p < 0.05$) than that of ^{177}Lu-AuNP ($15.5 \pm 1.7\%$ ID), whereas ^{177}Lu-RGD exhibited the highest tumor clearance ($5.7 \pm 0.8\%$ ID). Uptake occurred mainly in the kidneys and liver, as well as in the spleen, with negligible uptake in other organs. The mean tumor residence times were 61.6 ± 5.8 h (^{177}Lu-AuNP-RGD), 38.7 ± 4.1 h (^{177}Lu-AuNP) and 17.3 ± 2.4 h (^{177}Lu-RGD), while the mean kidney residence times were 0.88 ± 0.11 h (^{177}Lu-AuNP-RGD), 0.72 ± 0.10 h (^{177}Lu-AuNP) and 1.20 ± 0.24 h (^{177}Lu-RGD). Figure 5 shows the total radiation absorbed doses to the kidney, liver and spleen that were received during the different treatment protocols. The kidneys are the major dose-limiting

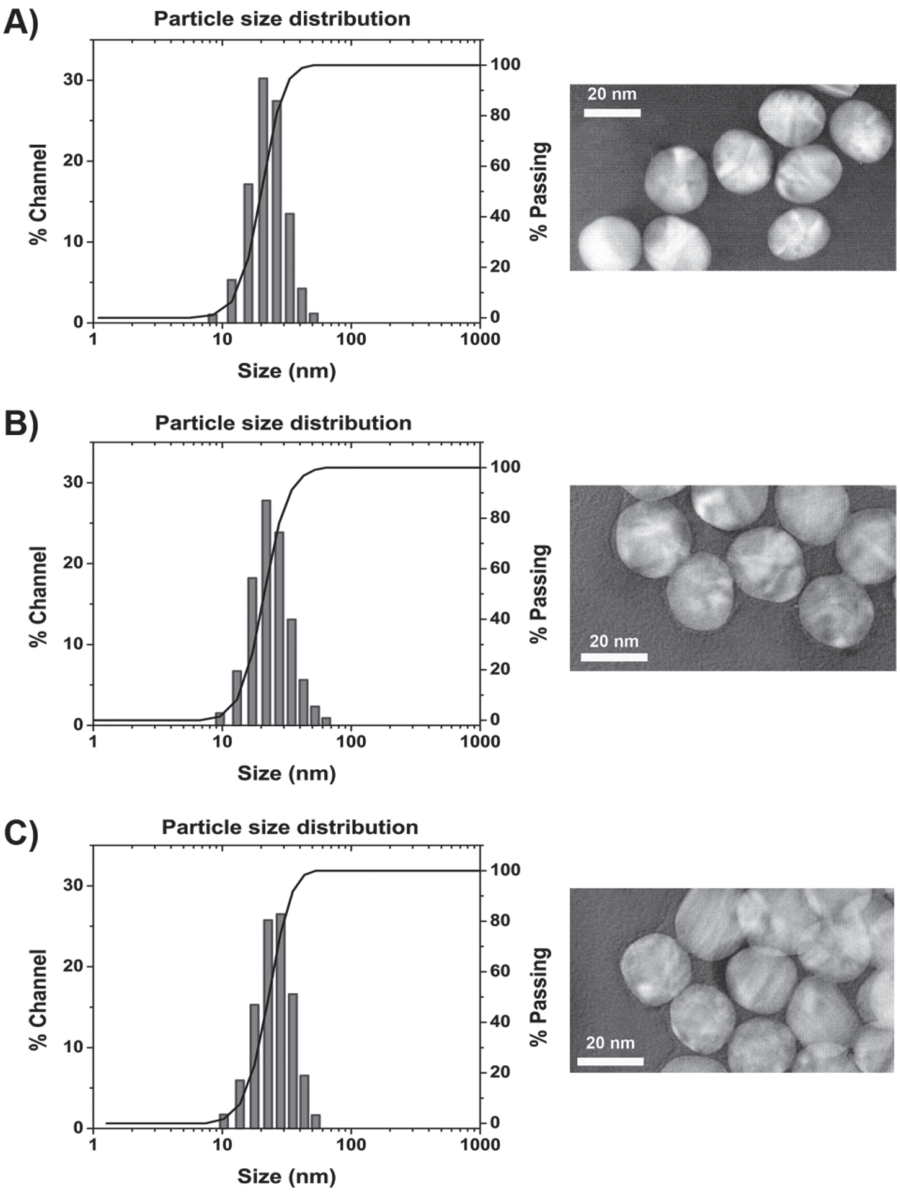

Figure 3. **TEM image and size distribution of (A) AuNP, (B) ^{177}Lu-AuNP and (C) ^{177}Lu-AuNP-RGD.**

organ because of the tubular re-absorption and retention of radioactivity, which may lead to radiation nephropathy.[22, 25] The maximum tolerated dose to the kidneys is 25–30 Gy and the dose in our study was less than 1.5 Gy in the three ^{177}Lu treatments.[22]

The tumor size progression for all ^{177}Lu-conjugates was significantly lower ($p < 0.05$) after 23 days with respect to that of the control group (Fig. 6). At 23 days, tumor size in the ^{177}Lu-AuNP-RGD group was 27 times smaller than that of the controls and twelve-fold and three-fold smaller than in the ^{177}Lu-RGD and ^{177}Lu-AuNP groups, respectively (Fig. 6). These tumor size data correlate with the doses delivered to the tumor in the following order: ^{177}Lu-AuNP-RGD (63.8 ± 7.9 Gy), ^{177}Lu-AuNP (38.3 ± 4.2 Gy) and ^{177}Lu-RGD (16.6 ± 1.3 Gy) (Fig. 6). The experimental protocol was completed at 23 days because the control mice presented tumor sizes as large as 3 g, therefore, sacrifice was necessary.

Figure 7 shows the ^{177}Lu-micro-SPECT/CT images at 24 h after the last injection (at 22 days of treatment), in which the differences in tumor sizes and radiopharmaceutical accumulation in cancer tissues as well as the negligible uptake in non-target organs are visible. The tumor area in which no radioactivity is observed is necrotic tissue. It is important to mention that in advanced stages, the histopathological features of glioma are extensive necrotic foci surrounded by tumor cells, while in less-advanced neoplasms the necrosis occurs sparsely. Because ^{177}Lu-AuNP-RGD induced less tumor progression than the other radiopharmaceuticals, its tumor uptake in the micro-SPECT/CT image was more homogeneous indicating less necrosis.

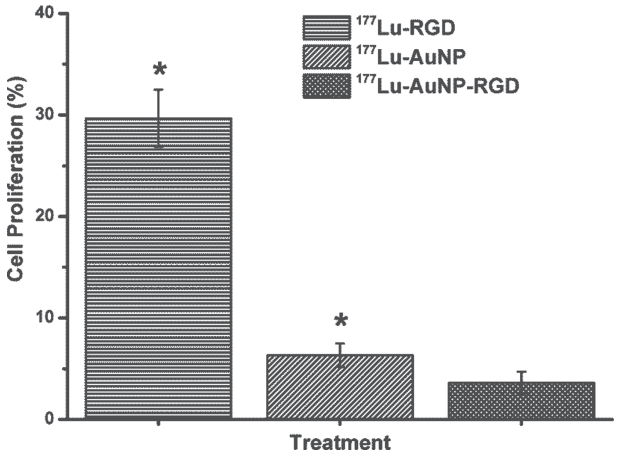

Figure 4. Effect of the ^{177}Lu-AuNP-RGD, ^{177}Lu-AuNP and ^{177}Lu-RGD on *in vitro* C6 cell proliferation. *Statistically significant difference ($p < 0.05$) versus ^{177}Lu-AuNP-RGD.

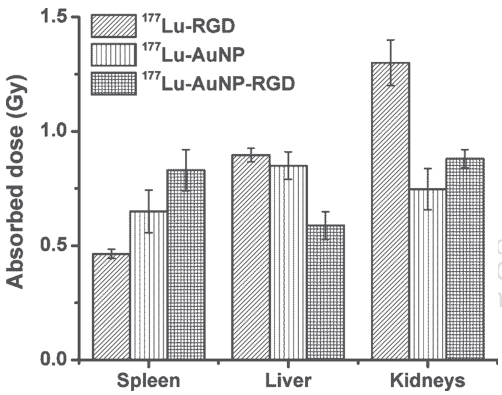

Figure 5. Radiation absorbed doses of ^{177}Lu-AuNP-RGD, ^{177}Lu-AuNP and ^{177}Lu-RGD to the spleen, liver and kidney induced in mice after 23 days of treatment.

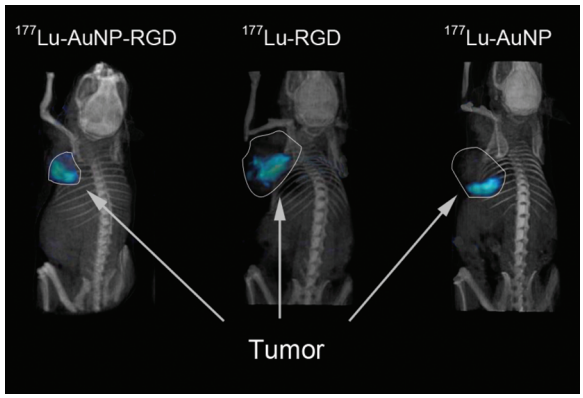

Figure 7. micro-SPECT/CT images of ^{177}Lu-AuNP-RGD, ^{177}Lu-AuNP and ^{177}Lu-RGD at 24 h after the last injection (at 22 days of treatment). The tumor areas in which no radioactivity is observed is necrotic tissue. Extensive necrotic foci are present in advanced stages of glioblastomas and in less-advanced neoplasms necrosis occurs sparsely. ^{177}Lu-AuNP-RGD tumor uptake is more homogeneous indicating less necrotic tissue.

Tumor Metabolic Activity

High accumulation of [^{18}F]FDG in the tumor and consequently high SUV values represent high metabolic activity in viable tumor cells. As shown in Table II, the SUV values of the groups treated with ^{177}Lu-radiopharmaceuticals were significantly lower than those of the control group ($p < 0.05$), while the SUV of the ^{177}Lu-AuNP-RGD group was significantly lower than that of ^{177}Lu-AuNP and ^{177}Lu-RGD groups ($p < 0.05$) (Fig. 8).

Histopathological Studies

Microscopic histological characteristics that define C6 gliomas were observed in tumors implanted in mice,

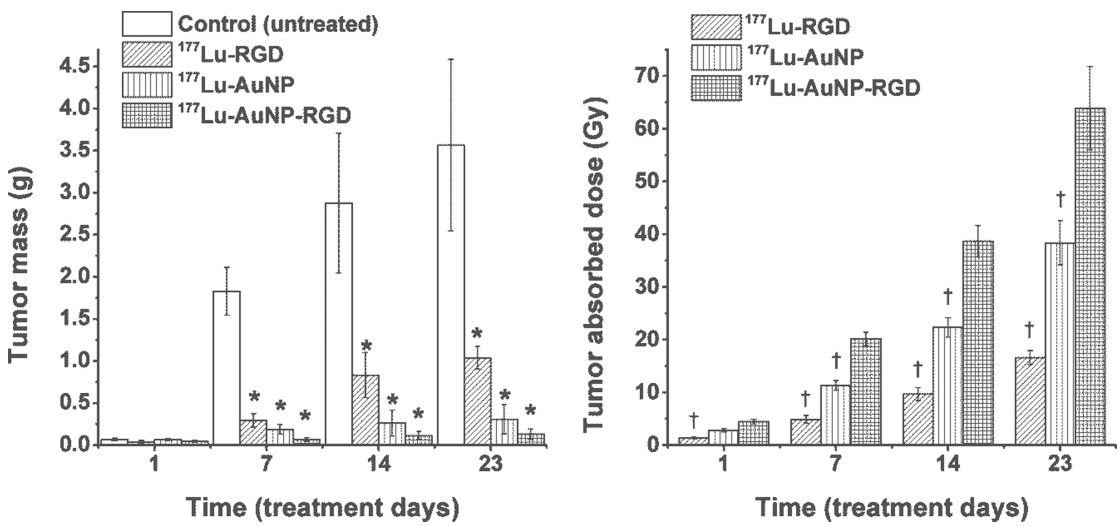

Figure 6. Tumor size progression for ^{177}Lu-AuNP-RGD, ^{177}Lu-AuNP and ^{177}Lu-RGD groups at different days of the treatment (left). The average radiation absorbed doses of ^{177}Lu-AuNP-RGD, ^{177}Lu-AuNP and ^{177}Lu-RGD delivered to C6 tumors (right). *Statistically significant difference ($p < 0.05$) versus control group. †Statistically significant difference ($p < 0.05$) versus ^{177}Lu-AuNP-RGD group.

Table II. Tumor metabolic activity (^{18}FDG standard uptake value, SUV), VEGF gene expression in tumor tissues (relative concentration versus β-actin) and urea, creatinine and urea nitrogen (BUN) serum concentrations in mice bearing C6 gliomas after 23 days of treatment with ^{177}Lu-AuNP-RGD, ^{177}Lu-RGD or ^{177}Lu-AuNP (mean ± standard deviation).

Treatment group	SUV	VEGF (RC)	Creatinine (mg/dL)	Urea (mg/dL)	BUN (mg/dL)
^{177}Lu-AuNP-RGD	0.335 ± 0.099*	0.012 ± 0.006*	0.230 ± 0.026	77.933 ± 7.497	30.417 ± 3.502
^{177}Lu-AuNP	0.584 ± 0.107*†	0.040 ± 0.012†	0.163 ± 0.050	67.025 ± 7.562	31.320 ± 3.534
^{177}Lu-RGD	2.740 ± 0.260*†	0.037 ± 0.006†	0.180 ± 0.036	59.267 ± 5.292	32.993 ± 2.433
Control	6.539 ± 0.052	0.070 ± 0.028	0.200 ± 0.057	63.550 ± 3.894	29.698 ± 1.821

Notes: *Statistically significant difference ($p < 0.05$) versus control (untreated group); †Statistically significant difference ($p < 0.05$) versus ^{177}Lu-AuNP-RGD group.

including giant cells and pleomorphic cell elements, mostly with vesicular nuclei and abundant eosinophil cytoplasm, mitotic forms and atypical nuclei. The following characteristics were observed in the different treatment groups.

^{177}Lu-AuNP-RGD: Tumors were delimited by a weak necrotic (*N*) area in the periphery (Fig. 9(A)); intratumoral vessels (*V*) observed in the necrotic zone were scarce and thinner than in other groups, with non-significant thick-wall (Figs. 9(B) and (C)); no inflammatory infiltrate was observed, and no detritus was formed in the tumor tissues.

^{177}Lu-RGD: Necrotic areas were surrounded and limited to the tumor periphery (Fig. 9(D)). Glomeruloid epithelial proliferations were occasionally present (Fig. 9(E)). Diffuse inflammatory infiltrate and cellular detritus were observed predominantly in necrotic sites, and intratumoral vessels were dispersed and occasional (Fig. 9(F)).

^{177}Lu-AuNP: Intratumoral thick-walled vessels were observed. Necrotic areas were dispersed in the periphery and within the tumor (Figs. 9(G) and (I)). In some cases, detritus accumulation and diffuse inflammatory infiltrate were present (Fig. 9(H)).

Control group: Extensive necrotic areas with pseudopalisading sections and thick-walled capillaries were observed (Figs. 9(J), (L)). The necrotic area exhibited more intratumoral vessels than in the ^{177}Lu-AuNP-RGD, ^{177}Lu-RGD or ^{177}Lu-AuNP groups. The vessel morphology was irregular in shape and size (Fig. 9(K)), and inflammatory infiltrate with an accumulation of cellular detritus was also observed (Fig. 9(L)).

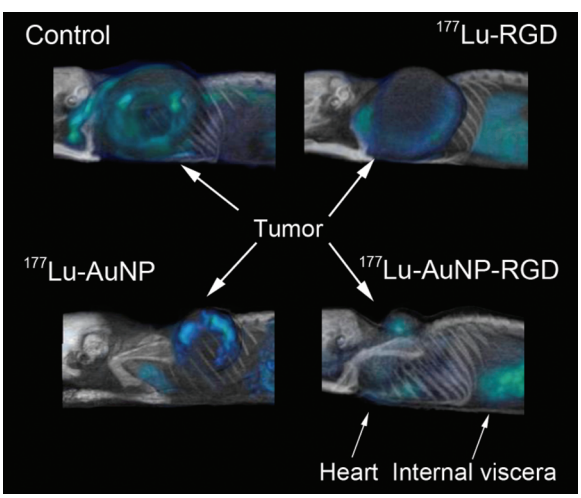

Figure 8. [^{18}F]FDG (2-deoxy-2-[^{18}F]fluoro-D-glucose)-micro PET/CT images of the control (untreated mouse), ^{177}Lu-AuNP-RGD, ^{177}Lu-RGD and ^{177}Lu-AuNP groups at 23 days of treatment. High accumulation of [^{18}F]FDG in the tumor represent high metabolic activity in the viable tumor cells.

No cytopathological damage was observed in kidneys. The glomerulus, proximal tube and distal tube exhibited no sign of necrosis or of damage any kind.

VEGF gene expression in tumor tissues. Real-time PCR analysis revealed that all treatments tended to reduce VEGF gene expression in tumor cells, although the effect in the ^{177}Lu-RGD group was not significant versus controls (Table II). However, treatment with ^{177}Lu-AuNP-RGD exerted the strongest and significant inhibition of VEGF gene expression when compared to the controls ($p < 0.05$). As ^{177}Lu-AuNP-RGD affinity for the $\alpha(v)\beta(3)$ integrin was demonstrated, the significant reduction in VEGF gene expression can be directly related to the $\alpha(v)\beta(3)$ blocking.[26]

Creatinine, urea and BUN quantification. Serum levels of creatinine, urea and BUN in the treatment groups were not statistically significant different with respect to control levels ($p > 0.05$) (Table II). This result correlates with the calculated low radiation absorbed dose to the kidneys, therefore, no renal toxicity was observed.

DISCUSSION

As expected, the radiopharmaceutical that yielded the greatest uptake and retention in tumors was ^{177}Lu-AuNP-RGD. The effects of this radiopharmaceutical can be attributed to passive and active-targeting mechanisms as well as multimeric and multivalent properties.[8] Consequently, the radiolabeled multimeric system delivered a greater radiation absorbed dose in tumors than did ^{177}Lu-AuNP or ^{177}Lu-RGD. The cRGD dose was also greater than that of ^{177}Lu-RGD, as ^{177}Lu-AuNP-RGD and ^{177}Lu-RGD were injected with the same cRGD concentration ($\sim 3 \times 10^{12}$ molecules of cRGD/50 μL). These results correlated with the observed therapeutic response in which ^{177}Lu-AuNP-RGD was the radiopharmaceutical that induced significantly less tumor progression, less tumor metabolic activity, fewer intratumoral vessels and reduced VEGF gene expression.

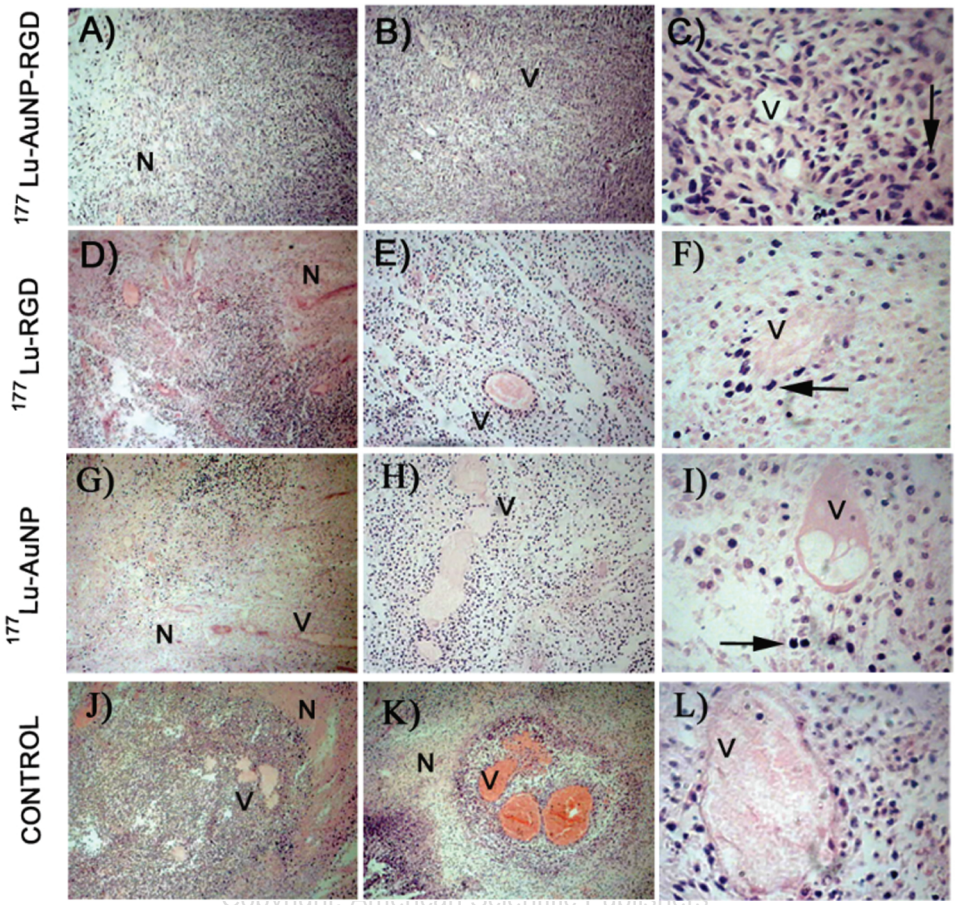

Figure 9. **Three microscopic views ((A), (D); (G), (B), (E), (H), (J), (K): ×100; (C), (F), (I), (L): ×200) of tumor histopathology with ^{177}Lu-AuNP-RGD, ^{177}Lu-RGD or ^{177}Lu-AuNP after 23 days of treatment. The control is a tumor from an untreated mouse. Less necrosis (*N*) and less vascular proliferation (*V*) in the ^{177}Lu-treatments against the control are observed. Nuclear pleomorphism is indicated by arrows.**

A peptide-nanoparticle conjugate bearing cRGD peptides provides a surface for simultaneous multiple interactions with the cell surface, giving rise to multivalent effects (defined as an affinity enhancement). Poethko et al.[24] reported that the minimum linker length is approximately 3.5 nm for the simultaneous binding of two c(RGD) motifs in the $\alpha(v)\beta(3)$ integrin. In the ^{177}Lu-AuNP-RGD system, the longest distance between two RGD motifs was calculated to be 11 nm, which is sufficiently long for the motifs to bind to adjacent $\alpha(v)\beta(3)$ integrins simultaneously.[8,12] The increase of peptide multiplicity in ^{177}Lu-AuNP-RGD may be at least partly responsible for the enhancement in tumor uptake (by an active-targeting mechanism) with respect to ^{177}Lu-RGD (^{177}Lu-DOTA-E-c(RGDfK)$_2$), in which the distance between the RGD molecules is 2.8 nm.[12]

Because the aim of this study was to evaluate and compare the therapeutic response, no tumor ablation was induced. However, in agreement with the radiation absorbed doses obtained in the non-target organs, the ^{177}Lu-AuNP-RGD dose could be increased ten-fold without exceeding the maximum tolerated radiation dose (MTD) to the kidneys (MTD = 25–30 Gy) or liver (MTD = 30–40 Gy), increasing the therapeutic efficacy and likely yielding complete tumor remission.[22,25]

The results indicated that ^{177}Lu-AuNP-RGD exerted the strongest and most significant inhibition of VEGF gene expression when compared to the controls ($p < 0.05$), potentially due to the multivalent RGD system, which may antagonize the function of the $\alpha(v)\beta(3)$ integrin, thereby inhibiting angiogenesis.[26] Cyclic RGD peptides have previously been reported to have limited activity as single agents in the treatment of glioblastoma, but when added to standard radiochemotherapy, appear to prolong progression-free and increase the overall survival in patients with newly diagnosed glioblastomas.[7] Therefore, the observed effect of ^{177}Lu-AuNP-RGD on VEGF gene expression could be due to the combined molecular targeting therapy (multimeric and multivalent RGD system) and radiotherapy (^{177}Lu) found in this one particular pharmaceutical.

Several trials have shown a significant improvement in clinical outcome when radiotherapy, chemotherapy or both were carried out under hyperthermic conditions in patients with advanced solid tumors such as cervical cancer.[27,28]

Hyperthermia increases the efficacy of radiotherapy by improving tumor oxygenation and interfering with DNA repair mechanisms.[27] In combination with chemotherapy, hyperthermia increases the drug concentration in the tumor area.[27] However, current techniques for hyperthermia induction display low spatial selectivity for the tissues that are heated. Lasers have been used for inducing hyperthermia, and spatial selectivity can be improved by adding gold nanoparticles to the tissue to be treated. By exposing nanoparticles to laser irradiation, it is possible to heat a localized area in tumors without any harmful heating of surrounding healthy tissues. The multifunctional ^{177}Lu-AuNP-RGD system prepared in this study, could also be used in photothermal cancer therapy using short NIR laser pulses to generate a second harmonic or a two-photon absorption process.[29] Second harmonic generation converts the NIR photons (800 nm) into visible photons (400 nm), which could be absorbed by the ^{177}Lu-AuNP-RGD nanospheres through surface plasmon and electron interband transition from the d band to the sp band with the consequent conversion of their energy into heat. NIR photons could also be directly absorbed and converted into heat through a nonlinear two-photon absorption process due to an aggregated alignment of the nanoparticles bound to cancer cells.[29,30]

If all the properties of the radiolabeled multifunctional system could be applied in nanomedicine, ^{177}Lu-AuNP-RGD could be potentially useful for the specific imaging of malignant tumors during treatment (SPECT imaging), for molecular targeting therapy/radiotherapy (multimeric RGD peptides plus high β-particle energy delivered per unit of targeted mass) and for photothermal therapy (localized heating). For therapeutic applications in humans, nanoparticles would have to be administered by an intratumoral injection or via a selective artery to avoid high uptake by organs of the reticuloendothelial system because of the colloidal nature of the nanoparticles.[31] Injection of the multimeric system into an artery of the affected organ would permit high uptake to a tumor and potentially to micrometastases or individual cancer cells.

CONCLUSIONS

^{177}Lu-labeled gold nanoparticles conjugated to cyclo-RGDfK(C) significantly decreased glioma tumor progression in mice through the effect of a combined molecular targeting therapy/radiotherapy. The inhibition of VEGF gene expression, involved in the angiogenesis process, indicated a molecular response. [^{18}F]fluor-deoxy-glucose-microPET/CT images showed a significant decrease in tumor metabolic activity. Therefore, ^{177}Lu-AuNP-RGD demonstrates properties suitable for use as an agent for molecular targeting radiotherapy.

Conflict of Interest

There are no conflicts of interest.

Author Disclosure Statement

No competing financial interests exist.

Acknowledgment: This study was supported by the Mexican National Council of Science and Technology (CONACYT-SEP-CB-2010-01-150942).

REFERENCES

1. D. L. Morse and R. J. Gillies, Molecular imaging and targeted therapies. *Biochem. Pharmacol*. 80, 731 (**2010**).
2. M. Patel, M. A. Vogelbaum, G. H. Barnett, R. Jalali, and M. S. Ahluwalia, Molecular targeted therapy in recurrent glioblastoma: current challenges and future directions. *Expert. Opin. Investig. Drugs* 21, 1247 (**2012**).
3. J. Kunikowska, L. Królicki, A. Hubalewska-Dydejczyk, R. Mikołajczak, A. Sowa-Staszczak, and D. Pawlak, Clinical results of radionuclide therapy of neuroendocrine tumours with ^{90}Y-DOTATATE and tandem ^{90}Y/^{177}Lu-DOTATATE: Which is a better therapy option?. *Eur. J. Nucl. Med. Mol. Imaging* 38, 1788 (**2011**).
4. R. Valkema, S. A. Pauwels, L. K. Kvols, D. J. Kwekkeboom, F. Jamar, M. de Jong, R. Barone, S. Walrand, P. P. Kooij, W. H. Bakker, J. Lasher, and E. P. Krenning, Long-term follow-up of renal function after peptide receptor radiation therapy with ^{90}Y-DOTA^0, Tyr^3-octreotide and ^{177}Lu-DOTA^0, Tyr^3-octreotate. *J. Nucl. Med.* 46, 83S (**2005**).
5. L. Bodei, M. Cremonesi, C. M. Grana, N. Fazio, S. Iodice, S. M. Baio, M. Bartolomei, D. Lombardo, M. E. Ferrari, M. Sansovini, M. Chinol, and G. Paganelli, Peptide receptor radionuclide therapy with ^{177}Lu-DOTATATE: The IEO phase I-II study. *Eur. J. Nucl. Med. Mol. Imaging* 38, 2125 (**2011**).
6. G. Ferro-Flores and C. A. Murphy, Pharmacokinetics and Dosimetry of ^{188}Re-pharmaceuticals. *Adv. Drug Deliv. Rev.* 60, 1389 (**2008**).
7. G. Tabatabai, J. C. Tonn, R. Stupp, and M. Weller, The role of integrins in glioma biology and anti-glioma therapies. *Curr. Pharm. Des.* 17, 2402 (**2011**).
8. S. Liu, Radiolabeled multimeric cyclic RGD peptides as integrin alphavbeta3 targeted radiotracers for tumor imaging. *Mol. Pharmaceutics* 3, 472 (**2006**).
9. S Liu, Radiolabeled cyclic RGD peptides as integrin $\alpha v \beta 3$-targeted radiotracers: Maximizing binding affinity via bivalency. *Bioconjugate Chem.* 20, 2199 (**2009**).
10. R. Haubner and C. Decristoforo, Radiolabeled RGD peptides and peptidomimetics for tumor targeting. *Front. Biosci.* 14, 872 (**2009**).
11. P. M. Mitrasinovic, Advances in $\alpha(\nu)\beta(3)$ integrin targeting cancer therapy and imaging with radiolabeled RGD peptides. *Curr. Radiopharm.* 2, 214 (**2009**).
12. X. Montet, M. Funovics, K, Montet-Abou, R. Weissleder, and J. Lee, Multivalent effects of RGD peptides obtained by nanoparticle display. *J. Med. Chem.* 49, 6087 (**2006**).
13. C. Huang, Q. Bao, D. Hunting, Y. Zheng, and L. Sanchez, Conformation-dependent DNA damage induced by gold nanoparticles. *J. Biomed. Nanotechnol.* 9, 856 (**2013**).
14. J. H. An, B. K. Oh, and J. W. Choi, Detection of tyrosine hydroxylase in dopaminergic neuron cell using gold nanoparticles-based barcode DNA. *J. Biomed. Nanotechnol.* 9, 639 (**2013**).
15. Y. Qu, Y. Huang, and X. Lü. Proteomic analysis of molecular biocompatibility of gold nanoparticles to human dermal fibroblasts-fetal. *J. Biomed. Nanotechnol.* 9, 40 (**2013**).
16. E. Morales-Avila, G. Ferro-Flores, B. E. Ocampo-García, L. M. De León-Rodríguez, C. L. Santos-Cuevas, R. García-Becerra, L. A. Medina, and L. Gómez-Oliván, Multimeric System of ^{99m}Tc-labeled Gold Nanoparticles Conjugated to c[RGDfK(C)] for Molecular Imaging of Tumor $\alpha(\mathrm{v})\beta(3)$ expression. *Bioconjugate Chem.* 22, 913 (**2011**).

17. M. Luna-Guitérrez, G. Ferro-Flores, B. E. Ocampo-García, N. Jiménez-Mancilla, E. Morales-Avila, L. de León Rodríguez, and K. Isaac-Olive, ^{177}Lu-labeled monomeric, dimeric and multimeric RGD peptides for the therapy of tumors expressing $\alpha(\mathrm{v})\beta(3)$ integrins. *J. Labelled Comp. Radiopharm.* 50, 140 (**2012**).

18. E. Morales-Avila, G. Ferro-Flores, B. E. Ocampo-García, and L. Gómez-Oliván, Engineered Multifunctional RGD-Gold Nanoparticles for the Detection of Tumour specific $\alpha(\mathrm{v})\beta(3)$ Expression: Chemical Characterisation and Ecotoxicological Risk Assessment. *J. Biomed. Nanotechnol.* 8, 991 (**2012**).

19. B. E. Ocampo-García, G. Ferro-Flores, E. Morales-Avila, and F. de M. Ramírez, Kit for Preparation of Multimeric Receptor-Specific ^{99m}Tc-Radiopharmaceuticals Based on Gold Nanoparticles. *Nucl. Med. Comm.* 32, 1095 (**2011**).

20. J. Rodriguez-Cortes, C. A. Murphy, G. Ferro-Flores, M. Pedraza-Lopez, and E. Murphy-Stack, Biokinetics and dosimetry with ^{177}Lu-DOTATATE in athymic mice with induced pancreatic malignant tumours: Preclinical studies. *Radiat. Eff. Defects Solids* 162, 791 (**2007**).

21. W. H. Miller, C. Hartmann-Siantar, D. Fisher, M. A. Descalle, T. Daly, J. Lehmann, M. R. Lewis, T. Hoffman, J. Smith, P. D. Situ, and W. A. Volkert, Evaluation of beta-absorbed fractions in a mouse model for ^{90}Y, ^{188}Re, ^{166}Ho,^{149}Pm, ^{64}Cu, and ^{177}Lu radionuclides. *Cancer Biother. Radiopharm.* 20, 436 (**2005**).

22. L. Bodei, M. Cremonesi, M. Ferrari, M. Pacifici, C. M. Grana, M. Bartolomei, S. M. Baio, M. Sansovini, and G. Paganelli, Long-term evaluation of renal toxicity after peptide receptor radionuclide therapy with ^{90}Y-DOTATOC and ^{177}Lu-DOTATATE: The role of associated risk factors. *Eur. J. Nucl. Med. Mol. Imaging* 35, 1847 (**2008**).

23. I. Olmedo, E. Araya, F. Sanz, E. Medina, J. Arbiol, and P. Toledo, How changes in the sequence of the peptide CLPFFD-NH_2 can modify the conjugation and stability of gold nanoparticles and their affinity for beta-amyloid fibrils. *Bioconjugate Chem.* 19, 1154 (**2008**).

24. T. Poethko, G. Thumshirn, U. Hersel, F. Rau, R. Haubner, M. Schwaiger, H. Kessler, and H. J. Wester, Improved tumor uptake, tumor retention and tumor/background ratios of pegylated RGD multimers. *J. Nucl. Med.* 44, 46P (**2003**).

25. E. Vegt, M. Jong, J. Wetzels, R. Masereeuw, M. Melis, W. J. Oyen, M. Gotthardt, and O. C. Boerman, Renal toxicity of radiolabeled peptides and antibody fragments: Mechanisms, impact on radionuclide therapy, and strategies for prevention. *J. Nucl. Med.* 51, 1049 (**2010**).

26. C. F. Montenegro, C. L. Salla-Pontes, J. U. Ribeiro, A. Z. Machado, R. F. Ramos, C. C. Figueiredo, V. Morandi, and H. S. Selistre-de-Araujo, Blocking $\alpha\mathrm{v}\beta 3$ integrin by a recombinant RGD disintegrin impairs VEGF signaling in endothelial cells. *Biochimie* 94, 1812 (**2012**).

27. M. Franckena, R. De Wit, A. C. Ansink, A. Notenboom, R. A. Canters, D. Fatehi, G. C. Van Rhoon, and J. Van Der Zee, Weekly systemic cisplatin plus locoregional hyperthermia: An effective treatment for patients with previously irradiated recurrent cervical carcinoma in a previously irradiated area. *Int. J. Hyperthermia* 23, 443 (**2007**).

28. M. Franckena, L. C. Lutgens, P. C. Koper, C. E. Kleynen, E. M. van der Steen-Banasik, J. J. Jobsen, J. W. Leer, C. L. Creutzberg, M. F. Dielwart, Y. van Norden, R. A. Canters, G. C. van Rhoon, and J. van der Zee, Radiotherapy and hyperthermia for treatment of primary locally advanced cervix cancer: Results in 378 patients. *Int. J. Radiat. Oncol. Biol. Phys.* 73, 242 (**2009**).

29. X. Huang, W. Qian, I. H. El-Sayed, and M. A. El-Sayed, The potential use of the enhanced nonlinear properties of gold nanospheres in photothermal cancer therapy. *Lasers Surg. Med.* 39, 747 (**2007**).

30. H. Mendoza-Nava, G. Ferro-Flores, B. Ocampo-García, J. Serment-Guerrero, C. Santos-Cuevas, N. Jiménez-Mancilla, M. Luna-Gutiérrez, and M. A. Camacho-López, Laser heating of gold nanospheres functionalized with octreotide: *In vitro* effect on HeLa cell viability. *Photomed. Laser Surg.* 31, 17 (**2013**).

31. N. Chanda, V. Kattumuri, R. Shukla, A. Zambre, K. Katti, A. Upendran, R. R. Kulkarni, P. Kan, G. M. Fent, S. W. Casteel, C. J. Smith, E. Boote, J. D. Robertson, C. Cutler, J. R. Lever, K. V. Katti, and R. Kannan, Bombesin functionalized gold nanoparticles show *in vitro* and *in vivo* cancer receptor specificity. *Proc. Natl. Acad. Sci. USA* 107, 8760 (**2010**).